ARTICLES
PUBLISHED ONLINE: 23 DECEMBER 2014 | DOI: 10.1038/NGEO2318
nature geoscience

Ocean rises are products of variable mantle composition, temperature and focused melting

Henry J. B. Dick[1]* and Huaiyang Zhou[2]*

Ocean ridges, where Earth's tectonic plates are pulled apart, range from more than 5-km depth in the Arctic to 750 m above sea level in Iceland. This huge relief is generally attributed to mantle plumes underlying mantle hotspots—areas of voluminous volcanism marked by ocean islands. The plumes are thought to feed the mantle beneath adjacent ocean ridges. This process results in thickened crust and ridge elevation to form ocean rises. The composition of mid-ocean ridge basalt, a direct function of mantle composition and temperature, varies systematically along ocean rises, but in a unique way for each different rise. Here we use thermodynamic calculations of melt-evolution pathways to show that variations in both mantle temperature and source composition are required to explain the chemical make-up of rise basalts. Thus, lateral gradients in mantle temperature cannot be uniquely determined from basalt chemistry, and ocean rises can be supported by chemically buoyant mantle or by robust mantle plumes. Our calculations also indicate that melt is conserved and focused by percolative flow towards the overlying ridge, progressively interacting with the mantle to shallow depth. We conclude that most mantle melting occurs by an overlooked mechanism, focused melting, whereas fractional melting is a secondary process that is important largely at shallow depth.

Since the pioneering work of Melson and others[1–3] it has been known that systematic along-axis variations in mid-ocean ridge basalt (MORB) major-element compositions exist. The full extent of these variations, and consistent explanations were first provided by Dick *et al.*[4], and Klein and Langmuir[5], who correlated them with proximity to hotspots, residual mantle composition[4] and ridge depth. They attributed these to variations in degree of mantle melting[4,5] and varying source composition[4]. MORB has since been widely used as a window into the Earth to infer variations in mantle temperature and crustal thickness—often ignoring the importance or even existence of lateral variations in upper-mantle major-element composition. Gale *et al.*[6] refining the analysis of Klein and Langmuir[5], again dismiss the importance of varying source composition relative to temperature, and estimate lateral upper-mantle temperature gradients of up to 200 °C. Here we show that mantle source composition plays a major role in determining MORB variability, and that estimates of upper-mantle temperature gradients ignoring varying source composition represent a maximum at best.

The most widely used MORB indicators are Klein and Langmuir's[5] $Na_{8.0}$ and $Fe_{8.0}$: basalt soda and iron content corrected for fractionation back to 8.0 wt% MgO (ref. 5). They attribute increasing $Fe_{8.0}$ to increasing mantle potential temperature and depth of melting, and decreasing $Na_{8.0}$ to increasing degree of melting and crustal thickness—with near-constant mantle source composition. Their work has led to wide use of $Na_{8.0}$ and $Fe_{8.0}$ as crustal thickness indicators and for geodynamic interpretation. There are, however, numerous problems with this approach. For example, following Klein and Langmuir's[5] interpretation, $Na_{8.0}$ at 12°–16° N on the Mid-Atlantic Ridge predicts crustal thickness of ~5 km and ~2,500-m ridge depth. However, the ridge is ~3,800 m deep, and mapping and sampling show that the crust consists of massive partially serpentinized peridotite intruded by gabbro plugs, with only scattered pillow basalt[7]. In addition, the correlation between $Na_{8.0}$ and depth in the Pacific is opposite that in the Atlantic and Indian oceans[8]. Alternatively, Niu and O'Hara[9] interpret varying $Na_{8.0}$–$Fe_{8.0}$ as largely due to changing mantle composition rather than temperature, and Presnall and Gudfinnsson[10] suggest that MORB is extracted at relatively constant temperature and pressure on the basis of experimental phase relations.

MORB major-element variations over rises

Ocean rises, ~28.0% of ocean ridges, are elevated sections that occur adjacent to mantle hotspots. Hotspots are regions of excess volcanism and volcanic islands for which plate tectonic theory has no explanation[11]. They are believed to be underlain by mantle plumes rooting below the asthenosphere that feed hot fertile mantle laterally to the adjacent ridge. This then results in thick crust and elevated topography along-axis. Recently Zhou and Dick[12] identified two classes of ocean rise. Axial rises are characterized by high melt flux and an axial high, and rifted rises by low melt flux, deep rift valleys, and abundant peridotite exposures[12,13]. Crustal thickness, a proxy for melt flux, varies from thin and discontinuous along the rifted Marion Rise, to 18.0 km near the Reykjanes Peninsula on the Icelandic axial rise[14]. There is no correlation between inferred melt flux and rise size; Marion and Icelandic rises being roughly equal in axial cross-section, one longer, and the other shallower. However, there may be a relationship between magma supply, overall rise depth and crustal thickness (Fig. 1).

Isotopes have provided the primary constraints on the nature of rises and hotspots (for example, refs 15–17). Rises, for example, generally have a depleted-MORB (ref. 18) baseline distal Sr-isotopic composition of 0.7026 (Fig. 1), while their proximal sections have unique enriched isotopic characters reflecting varying mantle source composition[19]. Although isotopes 'fingerprint' mantle sources, they are not as useful at telling how much mass and heat are involved. Major elements provide this. Mantle melting cannot vary much without consuming a lot of heat and moving a lot of mass. This provides a unique perspective on the origin and

[1]Woods Hole Oceanographic Institution, Woods Hole, Massachusetts 02543, USA. [2]State Key Laboratory of Marine Geology, Tongji University, Shanghai 200092, China. *e-mail: hdick@whoi.edu; zhouhy@tongji.edu.cn

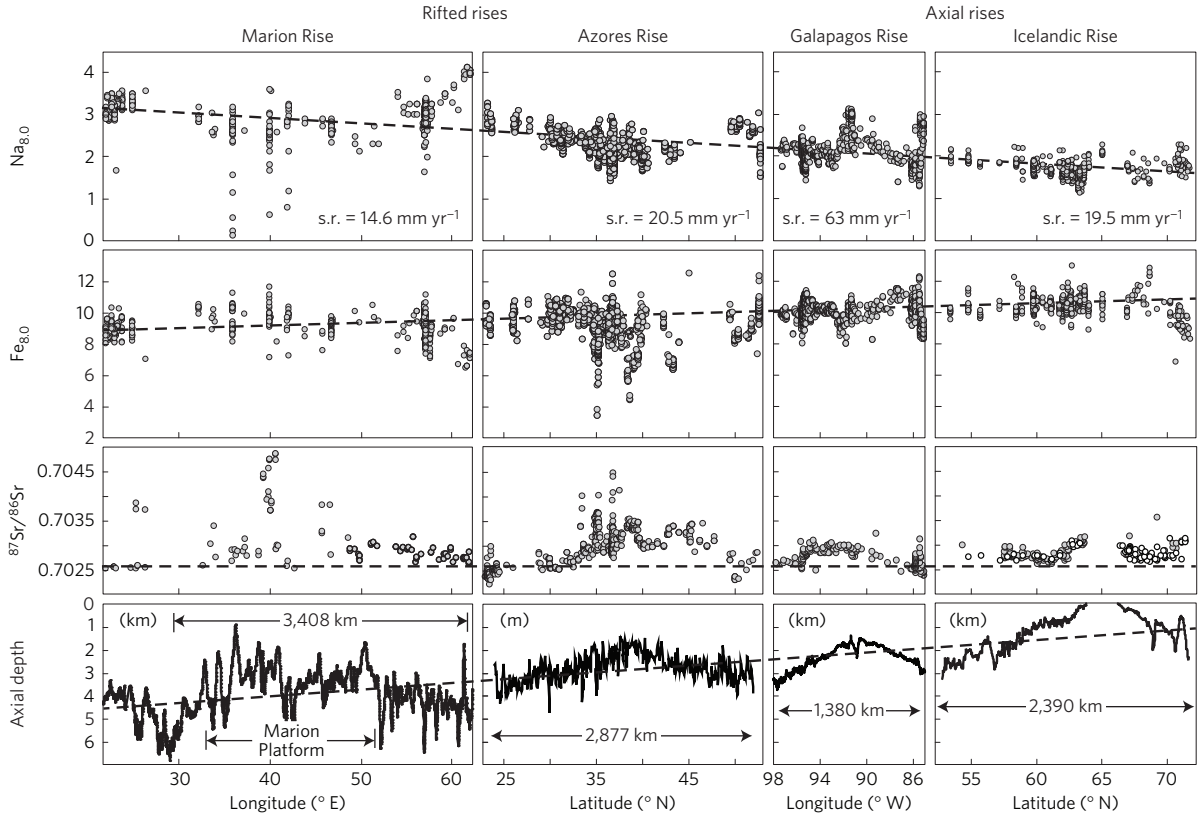

Figure 1 | $Na_{8.0}$, $Fe_{8.0}$, $^{8.07}Sr/^{8.06}Sr$ and depth along axis projected onto longitude or latitude for four major ocean rises. Depths and widths are all to scale. Data are from PetDB (http://www.earthchem.org/petdb) and Standish[48]. Ridge depths are from GeoMapApp (http://www.geomapapp.org). Dashed line shows the systematic ocean-rise global trend of $Fe_{8.0}$, $Na_{8.0}$ and rise height. Approximate spreading rate for each rise is indicated by s.r.

evolution of ocean rises; the major physiographic manifestations of 'plume'–ridge interaction and the nature of the Earth's upper mantle.

$Na_{8.0}$ and $Fe_{8.0}$ correlations with ocean rise depth exist; however, they are often quite different from the global ocean-ridge trend of negatively correlated $Na_{8.0}$ and $Fe_{8.0}$, and were generally excluded by Klein and Langmuir[5]. We believe rise trends are a fundamental manifestation of lateral major-element source heterogeneity. A necessary corollary of the mantle-plume hypothesis is the incorporation of large volumes of residual mantle into the asthenosphere, which can then become a regional MORB source. Similarly, delaminated lithosphere is compositionally buoyant and probably incorporated into the shallow asthenosphere during continental breakup. It is fundamentally illogical to find large along-axis variations in isotopic composition and not expect similar variations in bulk chemistry of the mantle. We find three scales of ocean-rise basalt variability: local, regional and global, which we address below.

Local trends[20] occur at the ridge-segment scale and are orthogonal to the Klein and Langmuir[5] ocean-ridge global trend, with individual basalt compositions defining linear arrays of positively correlated $Na_{8.0}$ and $Fe_{8.0}$ (ref. 20; Fig. 2). These have been explained as being due to melt extraction from different parts of the underlying melting column[20], to high pressure fractional crystallization[21], or to the decompression melting reaction ($Pyroxene + Melt_A \Rightarrow Olivine + Melt_B$; ref. 22).

Regional trends (Fig. 1), as defined here, occur at the scale of a rise. Along the Azores Rise, depth, $Na_{8.0}$ and $Fe_{8.0}$ follow Klein and Langmuir's[5] ocean-ridge global trend, predicting higher mantle potential temperature and thicker crust near the hotspot. At the Galapagos Rise $Na_{8.0}$ and $Fe_{8.0}$ correlate inversely, predicting the thinnest crust, shallowest melting, and lowest mantle temperature close to the hotspot opposite the predictions of Klein and Langmuir (ref. 5). On the Marion and Icelandic rises $Fe_{8.0}$ correlates poorly with little or no change, except adjacent the 204-km offset Jan Mayen Transform north of Iceland, where old lithosphere is juxtaposed against the ridge. Although there is little $Na_{8.0}$ variation over the Icelandic Rise, its strong depression over the Marion Rise would, following Klein and Langmuir[5], require higher degrees of melting, but at near-constant melting depth, even though the crust is thin or missing over large sections[12].

The ocean-rise global trend consists of a systematic variation from one rise to another in overall basalt composition (Figs 1 and 2), with a large shift in average $Na_{8.0}$ from ~3% to 1.8% and $Fe_{8.0}$ from 9% to 11%, corresponding to low and high magma budgets and increasing rise height. If this holds for other rises, it is a new trend that mimics the Klein and Langmuir[5] ocean-ridge global trend and probably has a related origin reflecting systematic changes in mantle temperature and composition. This is partially obscured in Fig. 2 as all data are plotted rather than averages. Although the depths of the ocean rises overlap from 1,500 to 3,000 m, their $Na_{8.0}$–$Fe_{8.0}$ fields differ significantly with virtually no overlap between the Marion and Reykjanes rises, with rifted rises having higher $Na_{8.0}$ at a given $Fe_{8.0}$. Thus, $Na_{8.0}$ cannot be used to predict ridge depth over at least a quarter of the ocean-ridge system.

Despite many apparent inconsistencies, $Na_{8.0}$–$Fe_{8.0}$ correlations over ocean rises convey significant information on the upper mantle and MORB generation. The question is why are the $Na_{8.0}$–$Fe_{8.0}$ rise trends so variable, and what controls them? Although the sodium content of mantle melts will systematically decrease with melting owing to dilution of an incompatible element, this is not the case for $Fe_{8.0}$. The behaviour of $Fe_{8.0}$ is explained by Klein and Langmuir[5] as being due to the expansion of the olivine phase field with decreasing pressure, which progressively reduces melt MgO and FeO (for example, ref. 23). As a melt percolating through the mantle would progressively equilibrate with it as it rose, thus eliminating any

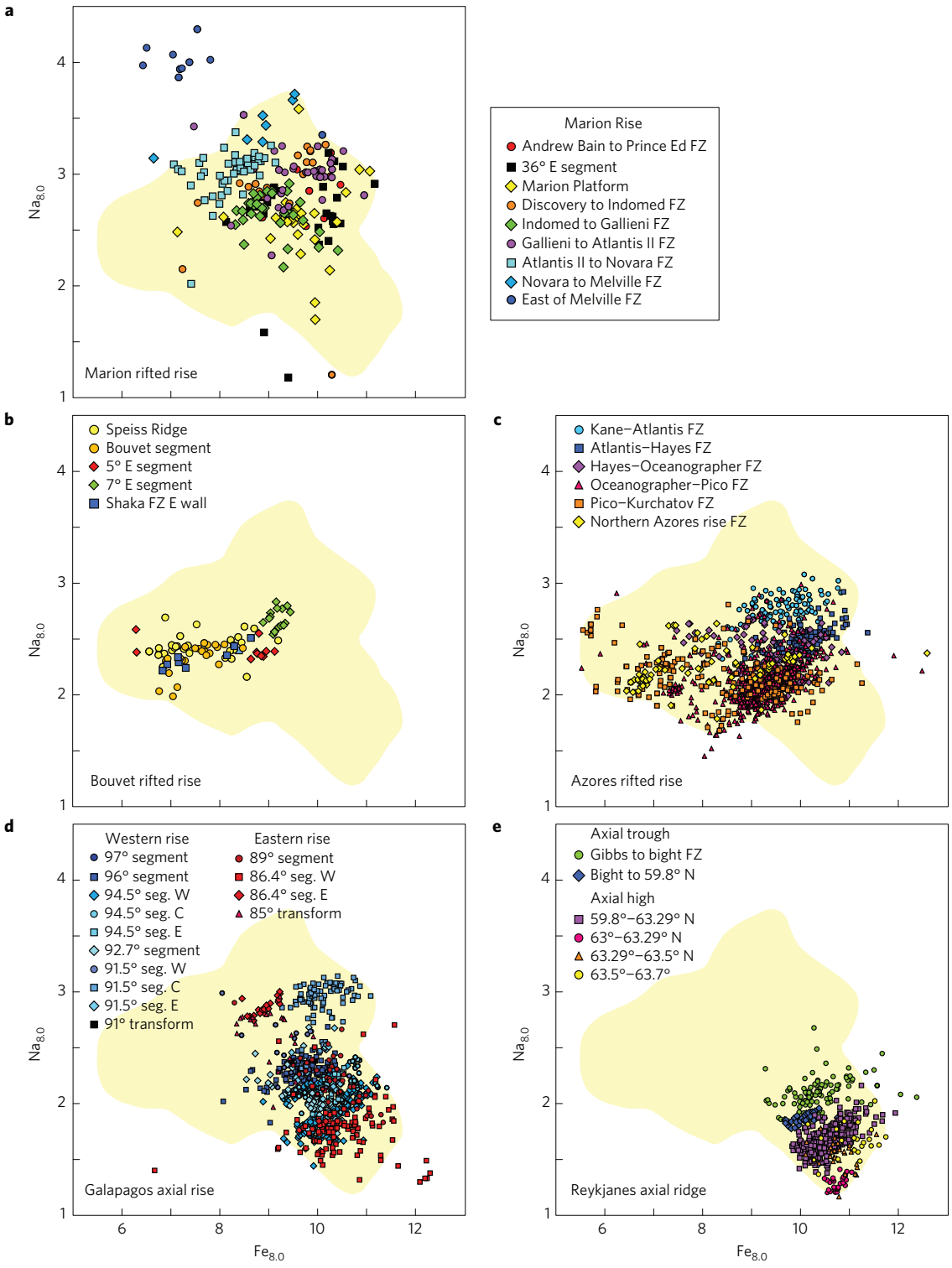

Figure 2 | $Na_{8.0}$ and $Fe_{8.0}$ plots for ocean rises. a, Marion Rise. **b**, Bouvet Rise. **c**, Azores Rise. **d**, Galapagos Rise. **e**, Reykjanes Rise. The last rise is the southern limb of the Icelandic Rise. Data sources as in Fig. 1. Yellow field represents the data for all 5 rises, excluding outliers, for comparison with the data for individual rises. Data symbols are coloured by ridge segment to highlight orthogonal local trends[20] that crosscut Klein and Langmuir's[5] ocean-ridge trend of negatively correlated $Na_{8.0}$ and $Fe_{8.0}$. Symbols are ordered in legends from south to north or west to east as appropriate. FZ, fracture zone.

pressure signal, Klein and Langmuir[5] appeal instead to averaging a series of melts from different depths, and creating a polybaric mix (pooled melt). Hence, the higher the $Fe_{8.0}$, the deeper melting begins, and the larger the volume of melt produced.

There are serious problems with both the Klein and Langmuir[5] and more traditional models based on simple phase relations that define specific depths of melt segregation (for example, ref. 24). These ignore abundant evidence in ophiolite and abyssal peridotites that magmas are highly reactive with the mantle up to the base of the crust, and therefore at least partially re-equilibrate with it, particularly with respect to Mg and Fe. Melt transport conduits are represented by dunites that formed by reaction between

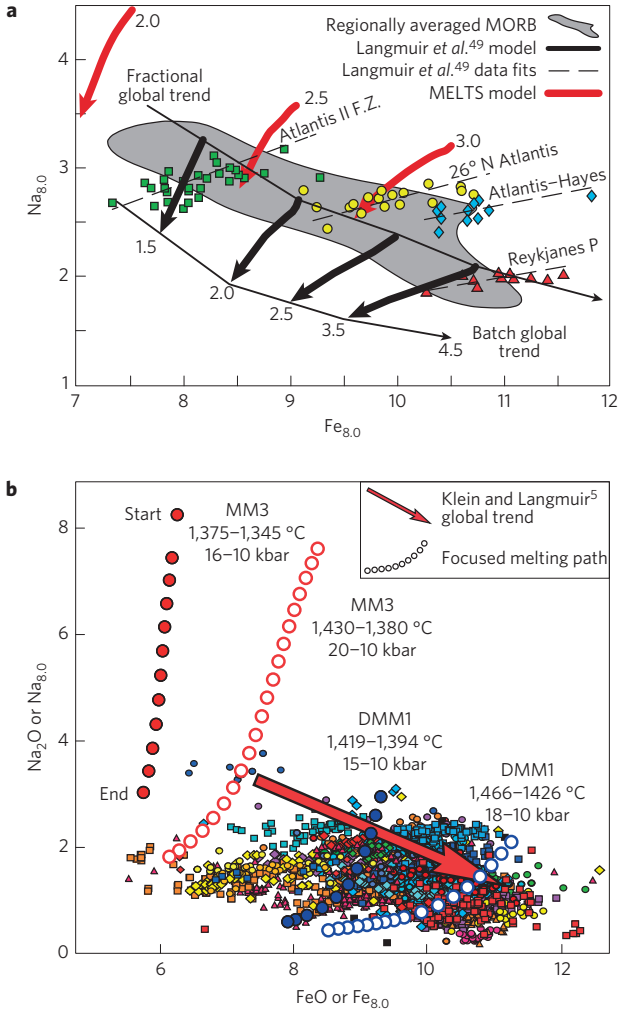

Figure 3 | Melting paths for MORB generation. a, Model for fractional followed by batch pooled melting modified from Asimow[29]. Light curves are fractional and batch-melting global ridge trends following Langmuir and colleagues[49]. Heavy black curves show batch melting from upper down to lower curve. Red curves calculated by MELTS (ref. 50). **b**, Focused-melting paths (FeO–Na_2O) for depleted DMM1 (ref. 38) and fertile MM3 (ref. 39) compositions. Ocean Rise $Na_{8.0}$–$Fe_{8.0}$ data are the same as in Fig. 2 retaining the same symbol colours. Repeated data symbols can be distinguished by comparison of the range of $Fe_{8.0}$ or $Na_{8.0}$ values for groups of symbols with those plotted in Fig. 2. Dots represent 0.5-kbar melting intervals and all calculations arbitrarily stopped at 10 kbar. Individual paths are labelled by initial and final melting *P* and *T*.

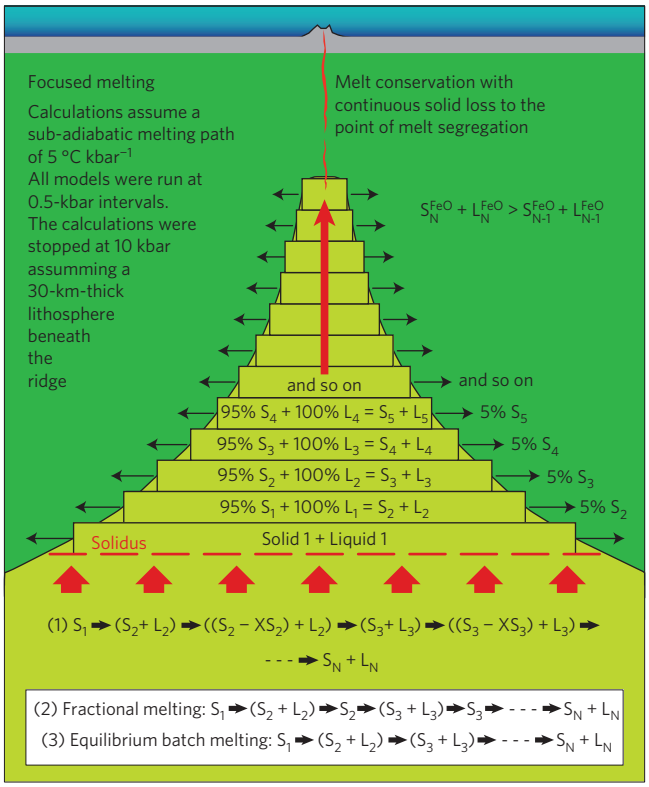

Figure 4 | Focused-melting model. Light green, asthenosphere; dark green, lithosphere; grey, crust; S, solid; L, melt. Melt velocity > mantle velocity. The model is calculated in steps to approximate reactive flow. As shown by equation (1), at each step the solid–liquid equilibrium is calculated, then 5% of the solid is removed and a new bulk composition calculated to begin the next step with 100% liquid retention. Transit effects through the lithosphere are not included in the model. Equations for fractional and equilibrium batch melting are shown in the inset for comparison.

the ascending melts and host mantle (for example, refs 25–28). Although there is strong evidence that the conduit melts are often not in equilibrium with shallow mantle[26], they form by dissolution and replacement of *in situ* pyroxene by olivine in the host peridotite. Moreover, olivine composition in the dunites and host peridotite is typically nearly identical: direct evidence that melts migrating up through the mantle interact with it even when focused to narrow channels. Thus, it is physically unrealistic to assume melts from different depths pool without their interacting and re-equilibrating with the mantle. Therefore, if $Fe_{8.0}$ is related to depth of melting, it is due to another mechanism.

Thermodynamic modelling of MORB and peridotite genesis

Asimow[29] earlier modelled $Na_{8.0}$–$Fe_{8.0}$ to explain the global and local ridge trends using MELTS (ref. 30), a thermodynamic potential-energy-minimization modelling program for calculating igneous phase equilibria[30]. The program is constrained by the limitations of available experimental data, but is useful for examining how changing parameters (*P*, *T*, f_{O_2} and so on) can affect magmatic systems. Asimow replicates the global-ridge $Na_{8.0}$–$Fe_{8.0}$ trend with fractional melting starting at a range of potential temperatures, and then aggregates the polybaric fractions along a batch-melting trend (Fig. 3a). However, this does not account for the fact that residual peridotites reflect fractional, not batch melting[31], and that the individual fractional trends emulate the orthogonal local trends only in their positive slope. These fractional paths cross ridge local trends at steep angles, becoming steeper with decreasing pressure. Moreover, the model fails to explain how the local trends are preserved after aggregation and mixing to produce the global-ridge trends.

The Asimow model is instructive, and presents the first internally thermodynamically self-consistent melt model for MORB major-element compositions. Building on Asimow's model, we formulate a somewhat different one that also attempts an internally thermodynamically consistent basis for $Na_{8.0}$–$Fe_{8.0}$ (Fig. 3b). Considering the idealized two-dimensional triangular melting regime beneath an ocean ridge, a good deal of mantle rock is removed from the melting column as the mantle rises up to the base of the crust; consistent with the evidence for focused flow of melt in the shallow mantle beneath ocean ridges (refs 32–34). Thus, models for MORB genesis must take this into consideration. This has been done for trace elements[35], and by Asimow and Stolper[36] for phase proportions in mantle residues, and here we do so for major-element compositions of melt and mineral residues.

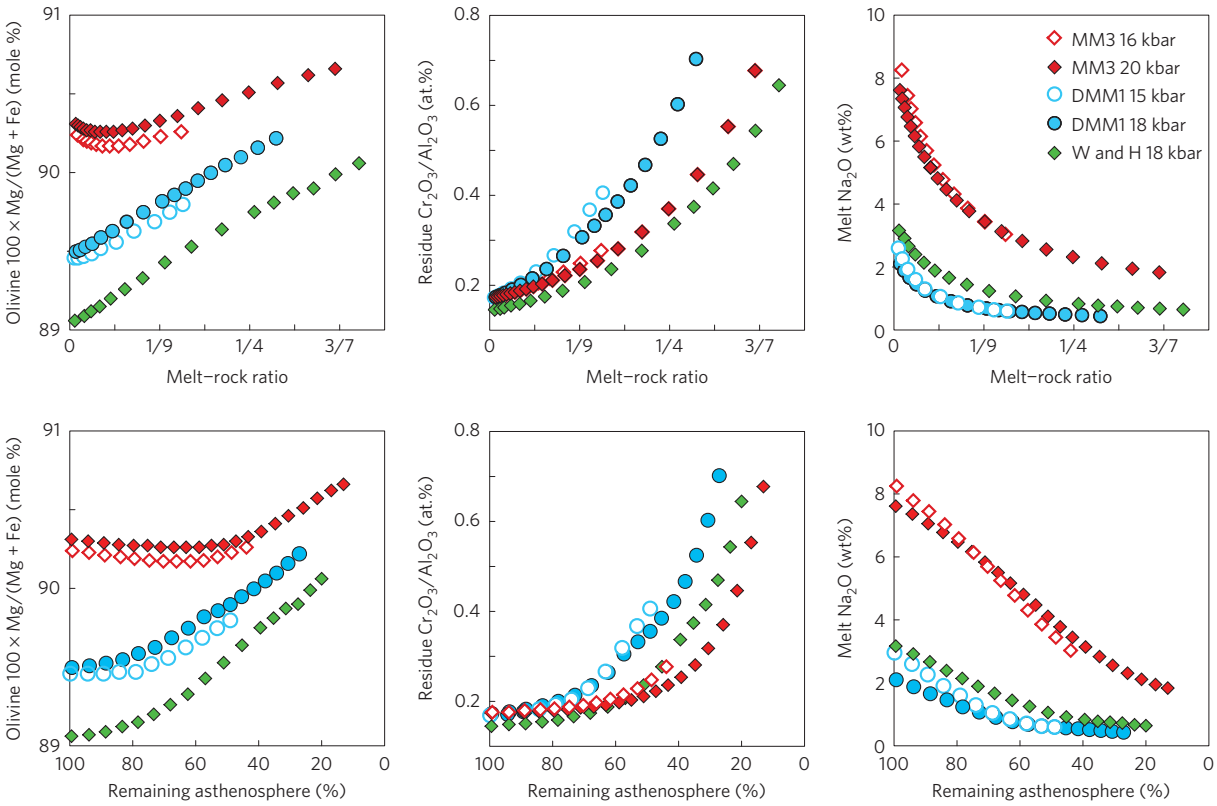

Figure 5 | Results of melt runs shown in Fig. 3b versus melt–rock ratio and remaining asthenosphere in the melting column. Melt–rock ratio is derived directly as the ratio of the percentage of melt to the percentage of solid calculated for each step, and is a direct analogue for total melt flux through the asthenosphere at any one point up to the last step in the calculation at 10 kbar. Remaining asthenosphere is the percentage of the original asthenospheric mass left in the melting column at each step in the calculation (S_n/S_1).

As iron is preferentially partitioned into the melt as it migrates up by reactive porous flow through an increasingly narrower melting zone the FeO content of the system must increase, even as the Mg×100/(Mg + Fe) is constrained by re-equilibration with the enclosing mantle. This is a major difference relative to simple batch or fractional melting models. Accordingly, the deeper the melting, the greater the $Fe_{8.0}$ of the final melt consistent with Klein and Langmuir's[5] original interpretation.

We computed melt-evolution paths for a focused-melting model using pMELTS, which is better calibrated for polybaric calculations than MELTS (ref. 37). For each path we started at a depth below the solidus for the potential temperature and bulk composition chosen, and arbitrarily stopped melting at 10 kbar. There is considerable debate over mantle source compositions, and to avoid this controversy we used the DMM1 (ref. 38) and MM3 (ref. 39) depleted and fertile compositions of the Stolper group. To approximate the mantle adiabat we used 5 °C kbar^{-1} following McKenzie and Bickle[40]. The computations were run by decompressing the bulk composition at one potential temperature until the melting point was reached, and then by melting at 0.5-kbar increments, at the end of each increment, we removed 5% of the solid residue, recalculated the bulk composition and then proceeded with the next step until we reached 10 kbar (Fig. 4).

Percentage of melting as conventionally used has little meaning here, unless you integrate melting over the entire melting column as done by Asimow and Langmuir[41] as there is no single mantle composition producing MORB in a triangular melting regime: rather mantle melting integrates melts derived from melting different degrees across a large mantle volume. Instead we plot two variables: melt–rock ratio, and remaining asthenospheric residue (Fig. 5). The former represents the amount of melt that passes through the mantle, and the latter gives the remaining percentage of the original mantle that crossed the solidus at the base of the mantle melting column at any step in the calculation. Although our calculation gives the proportions of melt and solid at each step, the melt proportion can be taken as the flux of melt through the section as mathematically one is equivalent to the other[36]. The absolute value of either parameter depends on the particular oxygen fugacity chosen, how it is controlled throughout the calculation, and the assumptions about how P and T vary with depth; however, the overall relationships shown remain robust over a wide range of conditions.

The effects of mantle temperature and composition

The results of our pMELTS calculations show that increasing initial potential temperature and a less fertile source composition both efficiently shift melt composition in the general direction of the $Na_{8.0}$–$Fe_{8.0}$ global-ridge trend for Fig. 3. However, unlike pooled melt models, the paths calculated for focused melting flatten downward at lower sodium, and where the degree of depletion is sufficient, align parallel to the basalt local trends. This provides a partial explanation for MORB local trends: that they represent local polybaric melt segregation into dunite melt transport conduits in the shallow mantle consistent with the hypothesis of Niu and Batiza[42].

pMELTS, although an improved version of MELTS, does not faithfully reproduce natural systems. In particular MgO contents in the calculated liquids are consistently 1–4% higher than expected based on olivine-melt partition coefficients, giving unrealistic values for Mg/(Mg+Fe). However, the model does explain several key aspects of MORB and mantle, which seems consistent with focused melting by reactive-percolative flow as a major component of the melt generation process.

Figure 3 shows that focused melting is required to realistically explain MORB major-element compositions, particularly the variations in $Fe_{8.0}$. Thus, fractional melting, required to explain the highly depleted trace-element composition of abyssal peridotites[35] probably occurs largely at shallow depths[43], as our model suggests, rather than dominating melt generation throughout the melting column. This is consistent with field observations that dunite melt transport channels ubiquitously crosscut shallow mantle mineral fabrics and late-formed layering (for example, refs 44–46), which is also consistent with theoretical calculations that show formation of dunite is difficult below 8 kbar (ref. 36). Nothing in our model, however, precludes polybaric melt segregation of individual batches of melt, which indeed may be required to explain the full isotopic and trace-element composition of MORB.

The varying $Na_{8.0}$–$Fe_{8.0}$ trends for ocean rises are easier to explain once source variation is included in the model. For example, the relatively short Galapagos and Icelandic orthogonal trends, higher $Fe_{8.0}$ and lower $Na_{8.0}$ (Fig. 2) indicate thinner lithosphere, and higher mantle potential temperatures, and thicker crust at axial rises than at the rifted rises. Decreasing $Fe_{8.0}$ and increasing $Na_{8.0}$ up the Galapagos Rise, however, imply a very different mantle source composition from Iceland, and probably a smaller increase in mantle temperatures with a more fertile source up the rise. The decreasing $Na_{8.0}$ up the Marion and Azores rifted rises, on the other hand, with geologic evidence for thin or missing crust up the former, and relatively thin crust up the latter[12], argue for an increasingly depleted mantle sources, although less so at the Azores, which with thicker crust and higher overall $Fe_{8.0}$, suggests higher baseline mantle temperatures.

The varying $Na_{8.0}$–$Fe_{8.0}$ trends for different ocean rises can be explained once source variation is included in the model. Thus, the anomalous high $Na_{8.0}$ at the Galapagos Rise crest can be explained by a source rich in low-melting components. This does not require a more fertile source; rather it could be an extremely depleted residue of an earlier melting event, for example, in an arc-mantle wedge, that is riddled with enriched veins recycled back to the asthenosphere. The flat $Fe_{8.0}$ over many ocean rises can reflect relatively constant potential temperature, particularly if the effects of water are included (for example, ref. 47), while the varying $Na_{8.0}$ reflects an increasingly depleted source up the rise as for the Marion Rise[12]. At Bouvet and the Azores $Na_{8.0}$–$Fe_{8.0}$ orthogonal trends extend to lower values than other rises. This can be explained by melting to shallower depth, or more extensive late-stage melt–rock reaction in a thicker lithosphere.

A 'new' endmember for mantle melting

Focused melting has generally been overlooked as a 'classic' endmember for melt generation. The significant differences are outlined in the equations in Fig. 4: focused melting represents conservation of melt, with continuous extraction of rock mass (equation (1)), fractional melting represents conserving rock mass with continuous extraction of melt (equation (2)), equilibrium batch melting occurs in a closed melt–rock system (equation (3)). Many variants of these models can be made, and none of these endmembers can represent the entire melt generation process without modification. The degree to which any one endmember controls the melting process probably depends on where in the melting/melt extraction column the observer looks. However, it is clear that focused melting by percolative flow as an endmember provides a thermodynamically consistent explanation for the variations in $Na_{8.0}$–$Fe_{8.0}$ along ocean ridges, and that initial mantle composition is as important as temperature in the generation of MORB. As the systematic variation in $Fe_{8.0}$ seems to be best explained by the percolative focused-flow model, this suggests in turn that most melts form in this manner, with fractional melting as a secondary process that becomes important at shallow depth, where melts segregate near the top of the mantle melting column.

Received 15 April 2014; accepted 12 November 2014; published online 23 December 2014

References

1. Melson, W. G., Vallier, T. L., Wright, T. L., Byerly, G. & Nelen, J. Chemical diversity of abyssal volcanic glass erupted along Pacific, Atlantic, and Indian Ocean sea-floor spreading centers. *Geophys. Pac. Ocean Basin Margin* **19,** 351–368 (1976).
2. Bryan, W. B. & Dick, H. J. B. Contrasted abyssal basalt liquidus trends: Evidence for mantle major element heterogeneity. *Earth Planet. Sci. Lett.* **58,** 15–26 (1982).
3. Schilling, J-G. *et al.* Petrologic and geochemical variations along the Mid-Atlantic Ridge from 29° N to 73° N. *Am. J. Sci.* **283,** 510–586 (1983).
4. Dick, H. J. B., Fisher, R. L. & Bryan, W. B. Mineralogic variability of the uppermost mantle along mid-ocean ridges. *Earth Planet. Sci. Lett.* **69,** 88–106 (1984).
5. Klein, E. M. & Langmuir, C. H. Global correlations of ocean ridge basalt chemistry with axial depth and crustal thickness. *J. Geophys. Res.* **92,** 8089–8115 (1987).
6. Gale, A., Langmuir, C. H. & Dalton, C. A. The global systematics of ocean ridge basalts and their origin. *J. Petrol.* **55,** 1051–1082 (2014).
7. Cannat, M. *et al.* Ultramafic and gabbroic exposures at the Mid-Atlantic Ridge: Geologic mapping in the 15° N region. *Tectonophysics* **279,** 193–213 (1997).
8. Small, C. & Danyushevsky, L. V. Plate kinematic explanation for mid-oceanic ridge depth discontinuities. *Geology* **31,** 399–402 (2003).
9. Niu, Y. & O'Hara, M. J. Global correlations of ocean ridge basalt chemistry with axial depth: A new perspective. *J. Petrol.* **49,** 633–664 (2008).
10. Presnall, D. C. & Gudfinnsson, G. H. Origin of the oceanic lithosphere. *J. Petrol.* **49,** 615–632 (2008).
11. Wilson, J. T. A possible origin of the Hawaiian Islands. *Can. J. Phys.* **41,** 863–870 (1963).
12. Zhou, H-y. & Dick, H. J. B. Thin crust as evidence for depleted mantle supporting the Marion Rise. *Nature* **494,** 195–200 (2013).
13. Ito, G. & Behn, M. D. Magmatic and tectonic extension at mid-ocean ridges: 2. Origin of axial morphology. *Geochem. Geophys. Geosyst.* **9,** Q09O12 (2008).
14. Weir, R. W. *et al.* Crustal structure of the northern Reykjanes Ridge and Reykjanes Peninsula, southwest Iceland. *J. Geophys. Res.* **106,** 6347–6368 (2001).
15. Schilling, J-G. Iceland mantle plume: Geochemical evidence along Reykjanes Ridge. *Nature* **242,** 565–571 (1973).
16. White, W. M., Schilling, J-G. & Hart, S. R. Evidence for the Azores mantle plume from strontium isotope geochemistry of the Central North Atlantic. *Nature* **263,** 659–663 (1976).
17. Hart, R., Dymond, J., Hogan, L. & Schilling, J-G. Mantle plume noble gas component in glassy basalts from Reykjanes Ridge. *Nature* **305,** 403–407 (1983).
18. Salters, V. J. M. & Stracke, A. Composition of the depleted mantle. *Geochem. Geophys. Geosyst.* **5,** Q05B07 (2004).
19. Zindler, A. & Hart, S. Chemical geodynamics. *Annu. Rev. Earth Planet. Sci.* **14,** 493–571 (1986).
20. Klein, E. M. & Langmuir, C. H. Local versus global variations in ocean ridge basalt composition: A reply. *J. Geophys. Res.* **96,** 4241–4252 (1989).
21. Kinzler, R. J. & Grove, T. Primary magmas of mid-ocean ridge basalts 2. Applications. *J. Geophys. Res.* **97,** 6907–6926 (1992).
22. Niu, Y. & Batiza, R. Chemical variation trends at fast and slow-spreading mid-ocean ridges. *J. Geophys. Res.* **98,** 7887–7903 (1993).
23. Kushiro, I. The system forsterite-diopside-silica with and without water at high pressures. *Am. J. Sci.* **267-A,** 269–294 (1969).
24. Presnall, D. C. & Hoover, J. D. Composition and depth of origin of primary mid-ocean ridge basalts. *Contrib. Mineral. Petrol.* **87,** 170–178 (1984).
25. Dick, H. J. B. *The Origin and Emplacement of the Josephine Peridotite* 400 PhD thesis, Yale Univ. (1976).
26. Dick, H. J. B. & Natland, J. H. in *Scientific Results* Vol. 147 (eds Gillis, K., Mevel, C. & Allan, J.) 103–134 (Texas A&M University, 1996).
27. Dick, H. J. B. & Natland, J. R. *An Offset Drilled Mantle Section: Evidence for Focused Melt Flow Beneath the East Pacific Rise from ODP Leg 147* Abstract vol. 25, 444 (Geological Society of America, 1993).
28. Kelemen, P. B., Shimizu, N. & Salters, V. J. M. Extraction of mid-ocean-ridge basalt from the upwelling mantle by focused flow of melt in dunite channels. *Nature* **375,** 747–753 (1995).
29. Asimow, P. D. A model that reconciles major- and trace-element data from abyssal peridotites. *Earth Planet. Sci. Lett.* **169,** 303–319 (1999).

30. Ghiorso, M. S. & Sack, R. O. Chemical mass-transfer in magmatic processes. 4. A revised and internally consistent thermodynamic model for the interpolation and extrapolation of liquid–solid equilibria in magmatic systems at elevated-temperatures and pressures. *Contrib. Mineral. Petrol.* **119,** 197–212 (1995).
31. Johnson, K. T. M., Dick, H. J. B. & Shimizu, N. Melting in the oceanic upper mantle: An ion microprobe study of diopsides in abyssal peridotites. *J. Geophys. Res.* **95,** 2661–2678 (1990).
32. Dick, H. J. B. in *Magmatism in the Ocean Basins, Geological Society Special Publication No. 42* (eds Saunders, A. D. & Norry, M. J.) 71–105 (Geological Society of London, 1989).
33. Dick, H. J. B., Tivey, M. A. & Tucholke, B. E. Plutonic foundation of a slow-spreading ridge segment: Oceanic core complex at Kane Megamullion, 23° 30′ N, 45° 20′ W. *Geochem. Geophys. Geosyst.* **9,** Q05014 (2008).
34. Sauter, D. *et al.* Focused magmatism versus amagmatic spreading along the ultra-slow spreading Southwest Indian Ridge: Evidence from TOBI side scan sonar imagery. *Geochem. Geophys. Geosyst.* **5,** Q10K09 (2004).
35. Spiegelman, M. Geochemical consequences of melt transport in 2-D: The sensitivity of trace elements to mantle. *Earth Planet. Sci. Lett.* **139,** 115–132 (1996).
36. Asimow, P. D. & Stolper, E. M. Steady-state mantle-melt interactions in one dimension: I. Equilibrium transport and melt focusing. *J. Petrol.* **40,** 475–494 (1999).
37. Ghiorso, M. S., Hirschmann, M. M., Reiners, P. W. & Kress, V. C. III The pMELTS: A revision of MELTS for improved calculation of phase relations and major element partitioning related to partial melting of the mantle to 3 GPa. *Geochem. Geophys. Geosyst.* **3,** 1–36 (2002).
38. Wasylenki, L. E., Baker, M. B., Kent, A. J. R. & Stolper, E. M. Near-solidus melting of the shallow upper mantle: Partial melting experiments on depleted peridotite. *J. Petrol.* **44,** 1163–1191 (2003).
39. Baker, M. B. & Stolper, E. M. Determining the composition of high-pressure mantle melts using diamond aggregates. *Geochim. Cosmochim. Acta* **58,** 2811–2827 (1994).
40. McKenzie, D. & Bickle, M. J. The volume and composition of melt generated by extension of the lithosphere. *J. Petrol.* **29,** 625–679 (1988).
41. Asimow, P. D. & Langmuir, C. H. The importance of water to oceanic melting regimes. *Nature* **421,** 815–820 (2003).
42. Niu, Y. & Batiza, R. Chemical variation trends at fast and slow spreading mid-ocean ridges. *J. Geophys. Res.* **98,** 7887–7902 (1993).
43. Kelemen, P. B., Hirth, G., Shimizu, N., Speigelman, M. & Dick, H. A review of melt migration processes in the adiabatically upwelling mantle beneath oceanic spreading ridges. *Phil. Trans. R. Soc. Lond. A* **355,** 283–318 (1997).
44. Dantas, C. *et al.* Pyroxenites from the Southwest Indian Ridge, 9–16° E; cumulates from incremental melt fractions produced at the top of a cold melting regime. *J. Petrol.* **48,** 647–660 (2007).
45. Dick, H. J. B., Lissenberg, C. J. & Warren, J. Mantle melting, melt transport and delivery beneath a slow-spreading ridge: The Paleo-MAR from 23° 15′ N to 23° 45′ N. *J. Petrol.* **51,** 425–467 (2010).
46. Warren, J. M. & Shimizu, N. Cryptic variations in abyssal peridotite compositions: Evidence for shallow-level melt infiltration in the oceanic lithosphere. *J. Petrol.* **51,** 395–423 (2010).
47. Asimow, P. D., Dixon, J. E. & Langmuir, C. H. A hydrous melting and fractionation model for mid-ocean ridge basalts: Application to the Mid-Atlantic Ridge near the Azores. *Geochem. Geophys. Geosyst.* **5,** Q01E16 (2004).
48. Standish, J. J. *The Influence of Ridge Geometry at the Ultraslow-Spreading Southwest Indian Ridge (9°–25° E): Basalt Composition Sensitivity to Variations in Source and Process* PhD thesis, Woods Hole Oceanographic Institution and the Massachusetts Institute of Technology (2006).
49. Langmuir, C. H., Klein, E. M. & Plank, T. in *Mantle Flow and Melt Generation at Mid-Ocean Ridges* Vol. 71 (eds Phipps Morgan, J., Blackman, D. K. & Sinton, J. M.) 183–280 (American Geophysical Union, 1992).
50. Ghiorso, M. S. Chemical mass transfer in magmatic processes I. Thermodynamic relations and numerical algorithms. *Contrib. Mineral. Petrol.* **90,** 107–120 (1985).

Acknowledgements

We would like to acknowledge M. Hirschman for his invaluable assistance in learning how to use pMELTS, input and criticism from E. Tursack, and numerous conversations on the subject with G. Gaetani, M. Behn, N. Shimizu, P. Kelemen, J. Natland and G. Hirth. P. Asimow, M. Ghiorso and V. Salters all provided helpful reviews that improved the manuscript both in clarity and thinking. Y. Liu and J. Wang checked our pMELTS calculations, using different conditions to test the robustness of our results. The National Science Foundation financially supported H.J.B.D. (NSF/OCE 08.0278.025). H.Z. would like to acknowledge the support of the Chinese National Key Basic Research Program (2012CB417300), China Ocean Mineral Resources Research and Development Association.

Author contributions

H.J.B.D. performed the initial modelling and wrote the paper with input from H.Z. H.Z. and his students carried out additional modelling for comparison to that presented in the paper to test the robustness of the conclusions. Interpretation of the results of the modelling and preparation of the figures and illustrations were performed jointly by the co-authors.

Additional information

Reprints and permissions information is available online at www.nature.com/reprints. Correspondence and requests for materials should be addressed to H.J.B.D. or H.Z.

Competing financial interests

The authors declare no competing financial interests.